



Optically transparent pectin/poly(methyl methacrylate) composite with thermal insulation and UV blocking properties based on anisotropic pectin cryogel

Fangxin Zou ^{a,1}, Hailong Li ^{b,1}, Yujiao Dong ^a, Girish C. Tewari ^a, Jaana Vapaavuori ^{a,*}

^a Department of Chemistry and Materials Science, Aalto University, Kemistintie 1, 02150 Espoo, Finland

^b Department of Physics, AlbaNova University Center, Stockholm University, 10691 Stockholm, Sweden



ARTICLE INFO

Keywords:

Pectin cryogel
Biocomposite
Optically transparent
Ultraviolet blocking
Thermal insulation

ABSTRACT

Bioderived polysaccharide-based cryogels prepared via freeze-casting method not only mimic the highly aligned anisotropic pore structure of plant stems but also offer other benefits as compared to biological structures, such as lower density, higher porosity, better permeability, and lower thermal conductivity. However, the application of polysaccharide cryogels to fabricate multifunctional composites is still at its infancy. In this study, a novel class of optically transparent pectin/poly(methyl methacrylate) (PMMA) composite (with optical transmittance as high as 84% and haze of 38% ~ 73%) combined with thermal insulation outperforming conventional glass has been prepared by using freeze-casted pectin cryogel as template. The final pectin/PMMA has comparable optical transmittance and comparable or lower haze as contrasted with most reported studies on transparent wood/bamboo. Astonishingly, this type of composite has very good UV blocking ability both as compared to glass and nanocellulose-based polymer composites. Overall, the optical properties of these composites can be optimized via controlling the pectin concentration and freeze-casting temperature. Furthermore, pectin/PMMA composites can reach much lower thermal conductivity (0.110 ~ 0.126 W/(m·K)) than glass. Therefore, these multifunctional pectin/PMMA composites could be beneficial in many applications, such as optically transparent materials, solar cell substrates, and UV protective displays.

1. Introduction

Highly anisotropic aligned porous structure present in the stems of natural plants provides many functionalities, such as mechanical strength and durability, as well as pathway for transmission of essential materials, such as water, ions, and nutrition. Inspired by natural plants, man-made materials mimicking biological anisotropic aligned porous structures open new opportunities to fabricate functional materials for various applications, for example, thermal insulation [1–3], energy storage/conversion [4–6], and water treatment [7–9]. A straightforward way of preparing bio-based anisotropic structures is to use natural wood to fabricate composites that combine optical transparency and good thermal insulation via infiltrating refractive index matched polymer into wood's porous structure [10–16]. However, for natural wood, harsh chemical treatments are needed either to remove [17] or modify [18–20] lignin that is a strong light absorber due to its many

chromophoric groups [21], or to functionalize the inner surface of wood pore wall prior to the infiltration of polymer to improve the molecular interactions between the wood cell wall and infiltrated polymer [13,22]. In addition, wood with low density is more suitable to fabricating transparent wood than high-density wood. This is due to the good permeability of low-density wood which ensures that polymers can be completely infiltrated into pore structure [23]. Overall, from the perspective of a material designer, employing wood wafers as templates for transparent wood applications encounters a natural limitation in available pore sizes, shapes and pore wall thicknesses.

To overcome the above-mentioned drawbacks, several techniques have been applied to fabricate anisotropic porous materials starting from solutions and suspensions, instead of wood wafers. Among all those techniques, freeze-casting (or ice-templating), which relies on the principle that ice crystal growth direction is controlled during freezing, is particularly outstanding to fabricate anisotropic porous materials

* Corresponding author.

E-mail address: jaana.vapaavuori@aalto.fi (J. Vapaavuori).

¹ These authors contributed equally to this work.

owing to its inexpensive, green, and simple freeze-drying process with lyophilization device [24]. This technique has been widely used to shape ceramics, synthetic polymers, and metals into anisotropic porous materials, commonly named as cryogels [24]. Due to the anisotropic structure, infiltration of polymers into these types of cryogels can significantly enhance the properties, such as thermal conductivity, electrical conductivity and solar energy conversion, of the resulting composites as compared to composites prepared from cryogels with randomly distributed pore structure [25]. For example, anisotropic boron nitride nanosheets (BNNS)/epoxy composite [26], used as thermal interface material, has higher thermal conductivity (6.07 W/(m·K)) than that of a composite prepared from randomly distributed structure (1.00 W/(m·K)).

Motivated by the urgent need to develop more sustainable materials economies, using natural raw materials with biodegradable, biocompatible, and non-toxic properties to fabricate functional composite materials has drawn an arising interesting. In recent years, various types of polysaccharides, such as cellulose [27,28], chitosan [29–31], chitin [32,33], and alginate [8,34,35], have been used to prepare cryogels with anisotropic pore structure via freeze-casting method. In addition to the highly aligned pore structure, these polysaccharide-based cryogels exhibit many advantageous properties compared to wood, such as lower density, higher porosity, and lower thermal conductivity [2]. Moreover, the big pores with pore sizes ranging from few tens to hundreds of micrometers endow cryogel a better permeability that allows for the facile infiltration of polymer into pores. The pore size can be tailored conventionally by varying the concentration and freezing temperature [36,37]. To the best of our knowledge, only a few works have reported the cellulose cryogel/polymer composites and most of them focused on the mechanical performance of the final composites [38–40]. However, cryogel/polymer composites made out of pectin cryogels have not been reported yet. Therefore, new ways of using polysaccharides cryogel to fabricate more functional composite materials are still needed, especially for pectin. Pectin is an inexpensive and abundant polysaccharide, which can be extracted from plant cell wall such as fruits peel/skin and sugar beet pulp [41–43] that are often considered as a side stream of food industry. Globally, 25 million tons of citrus peel [44], which contains 30 % pectin on dry basis [45], are produced as a byproduct per year. However, the established application of pectin is limited to a gelling and thickening agent in food industry [46]. Therefore, exploring new applications of pectin could open an opportunity to expand the industrial value of pectin with the increase of the commercial value of food industry byproduct, and increase the sustainability of functional composite fabrication by establishing new circular economy approaches.

In the present study, the possibility of fabricating optically transparent composite from pectin based cryogel with the infiltration of poly (methyl methacrylate) (PMMA, one of the widely used transparent plastics, chosen as a representative model system due to its refractive index matching with pectin) was investigated. In order to study the influence of the anisotropy of pectin cryogels on the optical properties of the final pectin/PMMA composite, three pectin concentrations, two freezing methods (freeze-casting and random freezing) and two freeze-casting temperatures (-79 °C (dry ice) and -196 °C (liquid nitrogen)) were used in this work. Optical transmittance and haze of these pectin/PMMA composites were measured and compared with those of reported transparent wood/bamboo. The thermal insulation properties of these pectin/PMMA composites were measured and compared with glass, PMMA, and reported transparent wood/bamboo. The pectin/PMMA composite with high optical transmittance, low haze, high UV blocking ability, and low thermal conductivity could be potentially used in optical, UV protective, and energy-efficient applications having the overall advantages of increased value of the byproducts, as well as easier and more environmentally-friendly process, as compared to transparent wood equivalents.

2. Experimental section

2.1. Materials

Pectin from citrus peel, methyl methacrylate (MMA, 99%), and 2,2'-azobis(2-methylpropionitrile) (AIBN, 98%) were purchased from Sigma-Aldrich. All chemicals were used without any further purification. Distilled water was used to dissolve pectin.

2.2. Preparation of pectin cryogels

Pectin cryogels were prepared with the following steps as illustrated in Fig. 1. Pectin solutions with various concentrations, from 1.5 wt% to 4.5 wt% (in dry weight), were first prepared by dissolving pectin powder in distilled water at room temperature for 24 h under magnetic stirring. Two types of freezing methods were applied to make pectin cryogels: freeze-casting and random freezing. For the freeze-casting method, half of the previously prepared pectin solution was poured into Teflon mode with copper as bottom plate. Then, the Teflon mode was transferred to and placed in the low temperature bath, which was filled with either dry ice (-79 °C) or liquid nitrogen (-196 °C), to get frozen gel. The left pectin solution was added in plastic sample tube and randomly frozen in the fridge at the temperature of -20 °C to obtain isotropic pore structure [37]. All the frozen gels were then freeze-dried for 7 days by using the Alpha 2-4 LSCbasic freeze dryer (Martin Christ Gefrier-trocknungsanlagen GmbH) to obtain pectin cryogels. The obtained pectin cryogels are named as "X wt%-N", where X is the pectin solution concentration and N is the freezing method/temperature.

2.3. Preparation of optically transparent Pectin/Poly(methyl methacrylate) (PMMA) composites

To prepare the optically transparent pectin/PMMA composites, the obtained pectin cryogel was first cut into small pieces with different thickness along the ice growth direction. Then the prepolymerized MMA solution was infiltrated into the pectin cryogel pieces, followed by the further polymerization of MMA in the oven at 75 °C for 4 h. The detailed processes are listed as follows: AIBN was mixed with MMA at 0.3 wt% weight fraction, then it was heated up to 75 °C and kept at this temperature for 25 min to get prepolymerized MMA solution. The prepolymerized MMA solution was then infiltrated into pectin cryogel pieces under vacuum at room temperature for 3 cycles. After the infiltration step, pectin cryogel piece infiltrated with prepolymerized MMA solution was sandwiched between two glass slides which were covered with aluminum foil and heated to 75 °C for 4 h in the oven for further polymerization of MMA to get pectin/PMMA composite. The pectin/PMMA composites are also named as "X wt%-N", where X is the pectin solution concentration and N is the freezing method/condition.

2.4. Characterization

2.4.1. Scanning electron microscope (SEM)

The morphologies of pectin cryogels and pectin/PMMA composites were characterized by Scanning Electron Microscope (TESCAN MIRA 3). Before the measurement, the sample's surface was coated by a thin Au/Pd (80/20) layer with Q150T coater (Quorum). The cryogels' pore wall density, which is based on the number of pore wall in 1 mm, and pore wall thickness were measured from SEM images by using ImageJ software.

2.4.2. Bulk density and porosity

Bulk densities (ρ_b) of pectin cryogels and the corresponding pectin/PMMA composites and the porosity of pectin cryogels were calculated as follows::

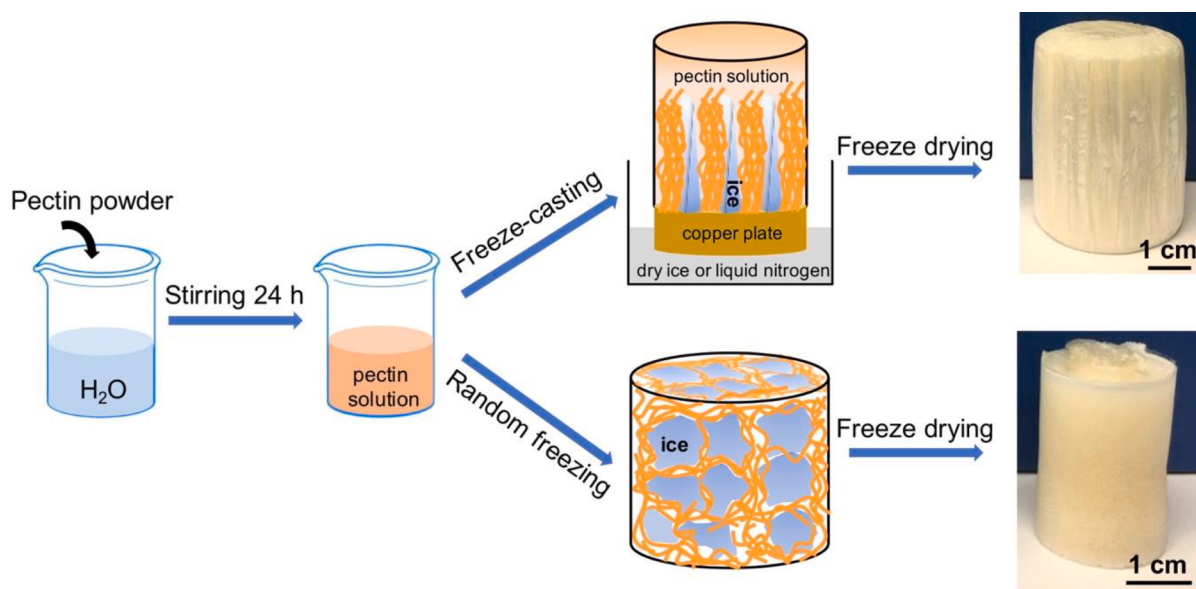


Fig. 1. Schematic illustration of the processing routes to prepare freeze-casted and randomly frozen pectin cryogels. The photos of the corresponding cryogels are presented on the right.

$$\rho_b = \frac{m}{V}$$

$$\text{Porosity} = \frac{\rho_s - \rho_b}{\rho_s} \times 100\%$$

where m and V are the sample's weight and volume, respectively. ρ_s is the skeletal density of pectin networks ($\rho_s = 1.5 \text{ g/cm}^3$) [47]. Sample's weight was measured by digital balance (Precisa 185 AM-FR). Sample's volume was calculated by $(\pi D^2) \times h \div 4$, where D is sample's diameter and h is sample's height. Both D and h were measured by digital caliper (Goobay, Germany). Each sample's weight, diameter, and height were measured for 4 times to obtain the average value and standard deviation.

2.4.3. Mechanical properties

Mechanical properties of the sample under tensile was measured by using Instron 4204 testing machine equipped with a 1 kN load cell and tensile rate at 5 mm/min. Before the measurement, all samples were kept under the condition of 23 °C and 50% humidity for 48 h. The Young's modulus was calculated from the initial linear region of strain–stress curves and obtained from 3 to 4 replicas per sample.

2.4.4. UV–Visible spectrometer

The optical properties (transmittance and haze) of pectin/PMMA composites were measured by UV-2600 with an ISR-2600 plus integrating sphere attachment (Shimadzu, Japan). Optical properties were measured from 200 nm to 800 nm and calculated as follows:

$$\text{Transmittance}(\%) = \frac{T_2}{T_1} \times 100\%$$

$$\text{Haze}(\%) = \left(\frac{T_4}{T_2} - \frac{T_3}{T_1} \right) \times 100\%$$

where T_1 , T_2 , T_3 , and T_4 are the background checking, total transmitted illumination, beam checking, and pure diffusive transmittance, respectively. Each sample was measured for 4 times to obtain the statistically reliable values. The average transmittance and haze were calculated from these 4 times measurements. UVA (320–400 nm) and UVB (290–320 nm) block percentages were also calculated as follows [48]:

$$\text{UVAblockpercentage}(\%) = 100\% - \frac{\int_{320}^{400} T(\lambda) d\lambda}{\int_{320}^{400} d\lambda} \times 100\%$$

$$\text{UVBblockpercentage}(\%) = 100\% - \frac{\int_{290}^{320} T(\lambda) d\lambda}{\int_{290}^{320} d\lambda} \times 100\%$$

where $T(\lambda)$ is the sample's average transmittance value, $d\lambda$ is the bandwidth, and λ is the wavelength.

2.4.5. Thermal insulation

The thermal conductivity measurements were performed on Physical Property Measurement System (PPMS DynaCool, Quantum Design) at room temperature. To obtain reliable thermal conductivity of glass and PMMA samples, silver nanowire glue was used to attach them in between two gold plated copper chips, then they were cured at 80 °C for 3 h to be used in the later thermal conductivity measurements. For pectin/PMMA composite samples, carbon tape was used to attach them in between copper chips to avoid the potential diffusion of silver nanowire glue into the nano pores in between pectin and PMMA layers (see SEM images in Results and discussion section). The thermal conductivity was measured at isothermal condition. At a fixed temperature a small amount of heat was applied to one face of a rectangular bar shaped sample. The temperature difference measured between two faces of the sample when the steady state was reached. By using sample dimensions (length, width, and thickness) and temperature difference, the thermal conductivity could be obtained. Thermal insulation performance during heating was measured by putting 2 mm thick sample sheet on 80 °C hot plate and the maximum surface temperature of each sample during heating was recorded by an infrared camera (PIR uc 180, InfraTec).

3. Results and discussion

From the photographs in Fig. 1 and SEM images in Fig. 2a and S1 (Supporting Information), it is evident that freeze-casting method endows the final cryogel with micropores aligned to the ice growth direction leading to anisotropic structure, whereas random freezing method results in final cryogel with randomly distributed micropores (isotropic structure). Similar anisotropic structure for the cryogels prepared via the freeze-casting method have already been reported for

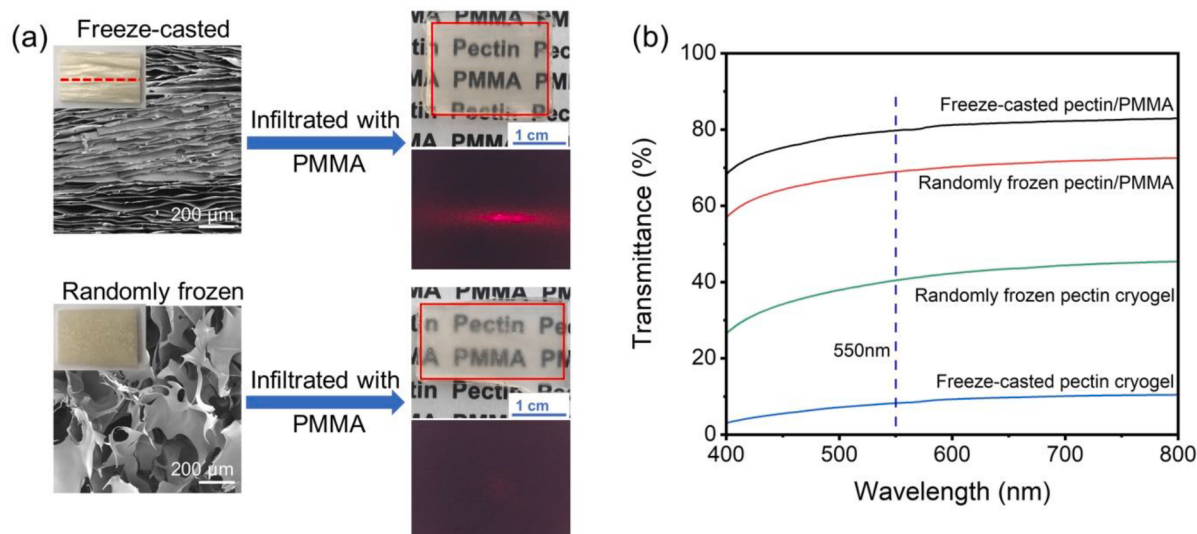


Fig. 2. SEM images of freeze-casted and randomly frozen pectin cryogels (cut along the ice growth direction or along the plastic tube) prepared from 3.0 wt% pectin solution (left panel of (a)). Photos of pectin cryogels before infiltration with PMMA are listed as inset. Red dash line in the inset indicates the ice growth direction. The photos of the 2 mm thick pectin/PMMA composite sheets on top of a printed symbol “Pectin PMMA” and the corresponding scattered laser spot photos (right panel of (a)). (b) Optical transmittance of the 2 mm thick pectin/PMMA composite sheets and the corresponding pectin cryogels.

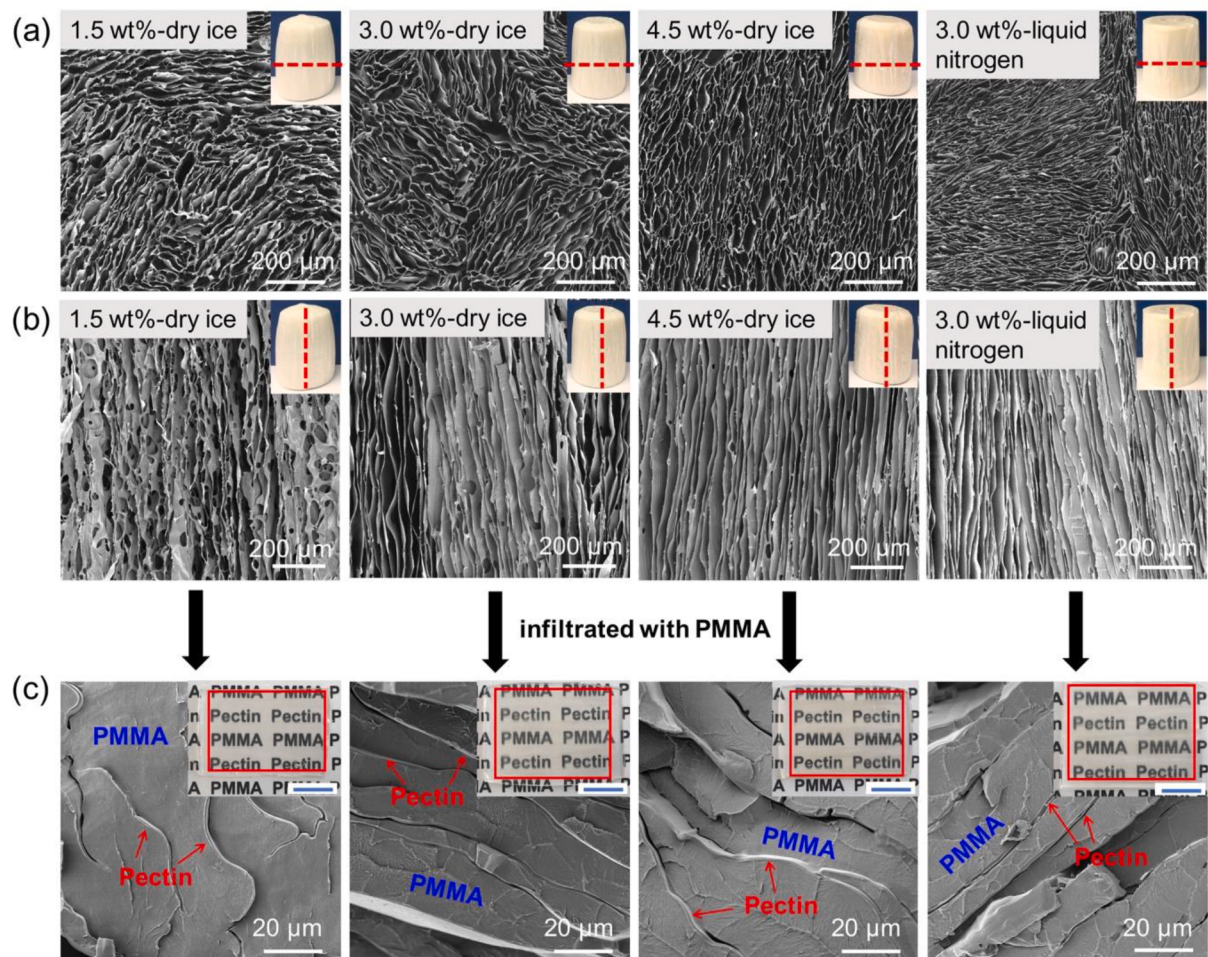


Fig. 3. SEM images of freeze-casted pectin cryogels (cut across (a) and along (b) the ice growth direction, respectively) prepared from different pectin concentration solutions and different freeze-casting temperature controlled by dry ice (-79 °C) and liquid nitrogen (-196 °C). The insets are the photos of the corresponding cryogels and the red dash line in the inset indicates the cutting direction. SEM images of pectin/PMMA composites (c). The insets are the photos of the corresponding 1.3 mm thick pectin/PMMA composite sheets on top of a printed symbol “Pectin PMMA”, scale bars are 1 cm.

some other polysaccharides [24], such as cellulose [49,50], chitosan [29,30], and alginate [8,34]. After the infiltration of PMMA, optically transparent pectin/PMMA composites were obtained for both freeze-casted and randomly frozen cryogels as shown from the photographs in the right panel of Fig. 2a. The transparency of the pectin/PMMA composite prepared from freeze-casted cryogel is higher than that prepared from randomly frozen cryogel over the whole spectrum of visible light. This conclusion is supported by the quantitative optical transmittance measured by UV-Vis presented in Fig. 2b. The 2 mm thick composite prepared from freeze-casted cryogel (black curve) has a higher transmittance (80 %) than that from randomly frozen cryogel (red curve, 69 %) at wavelength of 550 nm. Both transmittance values are much higher than the corresponding (non-infiltrated) pectin cryogels: 8 % and 40 % for freeze-casted and randomly frozen cryogels, respectively. This is due to the refractive index mismatch between PMMA (1.49) [15] and pectin (1.50) [51] being much smaller than that between air (1.0) and pectin (1.50), which reduces light scattering for the pectin/PMMA composites [15]. Additionally, due to the different morphologies of pectin cryogels before infiltration of PMMA, the prepared pectin/PMMA composites have different light scattering property. From the scattered laser spot photos (laser pointer bought from Deli Group Co., Ltd) in the right panel of Fig. 2a, it is observed that the laser light is scattered anisotropically for composite sheet prepared from freeze-casted cryogels and isotropically for composite sheet prepared from randomly frozen cryogels.

To elucidate the effect of the preparation parameters (pectin concentration and freeze-casting temperature) on the final properties of the freeze-casted pectin cryogels and the corresponding pectin/PMMA composites, three pectin concentrations (1.5, 3.0, and 4.5 wt%) and two freeze-casting temperatures (-79 °C and -196 °C) were selected to prepare the pectin cryogels. The SEM images of these freeze-casted pectin cryogels and the corresponding pectin/PMMA composites are shown in Fig. 3. All freeze-casted cryogels have anisotropic structures. Moreover, it is observed that both freeze-casting temperature and pectin concentration have influences on the pore wall density (Fig. S2). The average pore wall density of the pectin cryogels increases from 50 to 70 pore walls/mm when increasing the concentration of pectin solution from 1.5 wt% to 4.5 wt%. The most probable reason is that the increased viscosity due to the higher pectin concentration inhibits the growth of ice. This result is also consisted with the reported anisotropic pectin cryogels [37]. The freeze-casting temperature has more significant influence on the cryogel's pore wall density than pectin concentration. For

samples with pectin concentration of 3.0 wt%, the pore wall density increases from 60 to 127 pore walls/mm by decreasing the freeze temperature from -79 °C (dry ice) to -196 °C (liquid nitrogen) due to the more rapid freezing at lower temperature. After the infiltration of PMMA into pectin cryogel's pores, it is observed that all the pores in the pectin cryogels were fully and homogeneously filled with PMMA (Fig. 3c) and all composites are optically transparent (inset in Fig. 3c). This is due to the low density (0.019 g/cm³ – 0.053 g/cm³) and high porosity (> 96%) of pectin cryogel (Table S1, Supporting Information), which endow cryogel with a better permeability that allows for the infiltration of polymer into pores. Although, the final pectin/PMMA composites have slightly lower densities (1.03–1.09 g/cm³, Table S1, Supporting Information) than pure PMMA [15] (around 1.15 g/cm³), they still have comparable mechanical properties with pure PMMA (Fig. S3).

Interestingly, an anisotropic pore orientation is observed for the pore cross-section of all the cryogels from the SEM images in Fig. 3a even for a small scanning area. Analogously, larger areas of the cryogels consist of areas of different pore orientations, as indicated by different colored areas in SEM images presented in Fig. 4a-d. From these SEM images marked with different pore orientation, it is observed that the obtained cryogel has higher pore section anisotropy when increasing the pectin concentration from 1.5 wt% to 4.5 wt%, as the growth of ice crystals is affected by the viscosity of the pectin solution [37]. This is consisted with the reported anisotropic pectin cryogels [37]. This conclusion is also supported by the scattered laser spot photos in Fig. 4a'-c', where the light has been scattered anisotropic more and more with increasing the pectin concentration (Fig. 4a'-4c'). This anisotropic light scattering was also observed for the composite prepared from liquid nitrogen freeze-casted cryogel (Fig. 4d') and it has higher anisotropic light scattering than that of composite prepared from dry ice freeze-casted cryogel at the same pectin concentration (Fig. 4b'). It is most likely caused by the fast-freezing process in which many parallel and small pores were formed for liquid nitrogen freeze-casted cryogel. In addition, future work could consist of applying bidirectional freezing technique to fabricate pectin cryogel having highly ordered anisotropic structure and the corresponding cryogel/polymer composites.

To investigate the effect of the morphology of the initial cryogels on the optical properties for the composites, the optical transmittance of pectin/PMMA composite sheets with different thickness (1.3 mm, 2 mm, and 3.1 mm) were measured and plotted in Fig. 5a, S4a, and S4c. It is observed that the optical transmittance (at wavelength of 550 nm) decreases when increasing the pectin concentration from 1.5 wt% to 4.5 wt

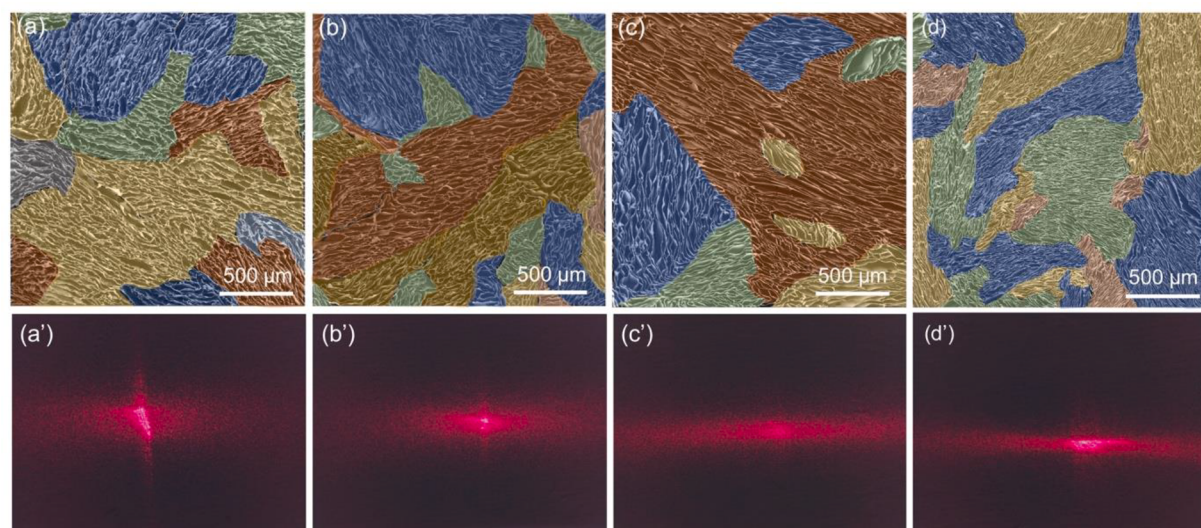


Fig. 4. Low magnification SEM images of freeze-casted pectin cryogels (cut across the ice growth direction) with pectin concentration of 1.5 wt% (a), 3.0 wt% (b), 4.5 wt% (c), and 3.0 wt%-liquid nitrogen (d). Different colored areas are marked to indicate the different pore orientations. The scattered laser spot photos (a', b', c', and d') of the corresponding 3 mm thick pectin/PMMA composite sheets.

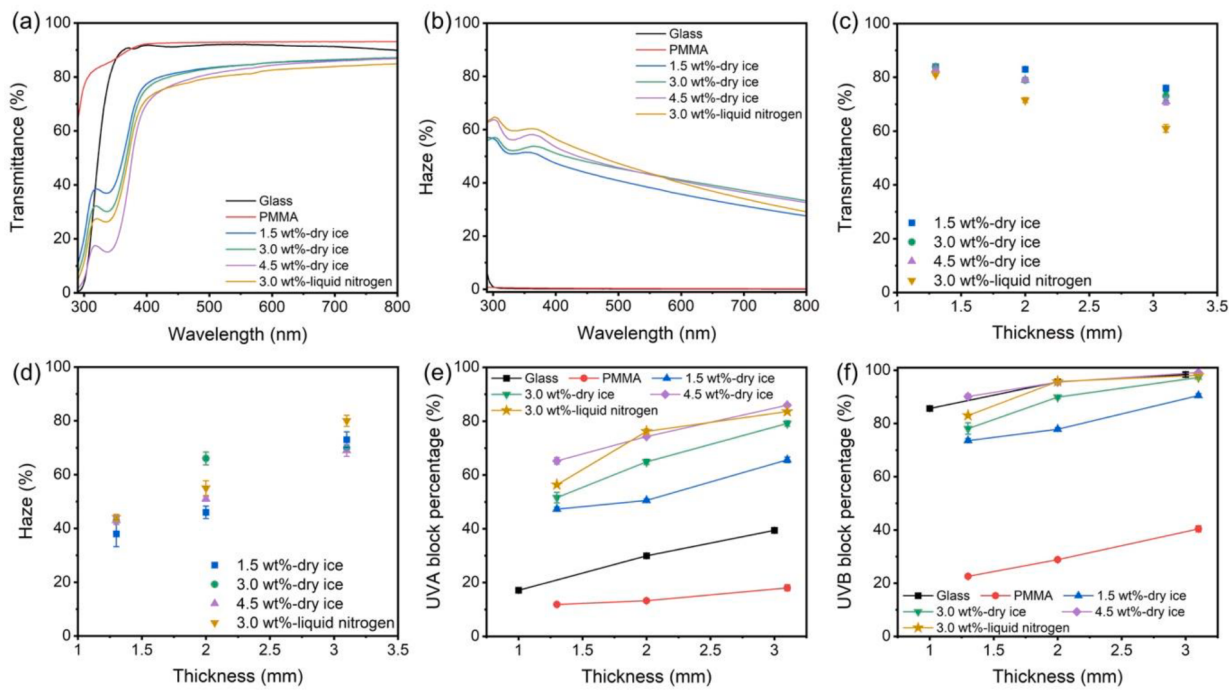


Fig. 5. Optical transmittance (a) and haze (b) of the 1.3 mm thick pectin/PMMA composite sheets prepared from freeze-casted cryogels with different pectin concentration solutions and different freeze-casting temperature. The transmittance and haze of 1.3 mm thick PMMA sheet and 1.0 mm thick glass are added in (a) and (b) as references. Optical transmittance (c) and haze (d) at wavelength of 550 nm as a function of pectin/PMMA composites' thickness. UVA block percentage (e) and UVB block percentage (f) as a function of thickness for glass, PMMA, and pectin/PMMA composites. If the errors are not seen, they are smaller or equal to the symbol.

%. This can be addressed to two reasons. Firstly, the composite with higher pectin concentration has higher density of polymer/pectin interface due to the higher pore wall density of the initial cryogels, which results in the increasing of scattering. The other reason is that the weak absorption at 550 nm is slightly enhanced when the pectin content is increased. This absorption enhancement is more obvious for the UV-Vis light absorption at around 340 nm (Fig. 5a) due to significantly higher absorption coefficient of pectin at that wavelength. Therefore, the more pectin in the cryogel, the more pronounced yellow color of the pectin/PMMA composite. This is consisted with the color of the photographs in Fig. 3c, where the composite prepared from pectin concentration of 1.5 wt% is almost colorless, while the yellow color of composite has been enhanced when the pectin concentration increases from 1.5 wt% to 4.5 wt%. Moreover, freeze-casting with liquid nitrogen results in the corresponding composite with the lowest optical transmittance. This is due to the highest density of polymer/pectin interface caused by the highest pore wall density compared to the other pectin cryogels freeze-casted with dry ice.

The optical haze is used to quantify the scattering of the transmitted light which passes through the sample. The stronger the light scattered in the forward direction, the higher the haze. The optical haze of pectin/PMMA composite sheets with different thickness are presented in Fig. 5b, S4b, and S4d. It is observed that the optical haze increases with increasing pectin concentration and decreasing the freeze-casting temperature. This can be attributed to the higher pectin concentration and lower freeze-casting temperature resulting in the higher density of polymer/pectin interface which leads to the light being reflected and transmitted in the sample with a longer pathway, thus being scattered more.

The thickness dependences of optical transmittance and haze (at wavelength of 550 nm) for all the pectin/PMMA composites are shown in Fig. 5c and 5d, respectively. As the thickness increases, the optical transmittance decreases only slightly, while the optical haze increases significantly. This is due to the longer light pathway and the increased

scattering centers with increasing thickness. These results are consistent with the reported transparent wood [52] and transparent bamboo [53]. Interestingly, the thickness dependence of optical transmittance is more sensitive with the freeze-casting temperature than the pectin concentration. For example, with increasing thickness from 1.3 mm to 3.1 mm, the optical transmittances at 550 nm of the composites prepared from dry ice freeze-casted cryogels with pectin concentration of 1.5 wt%, 3.0 wt%, and 4.5 wt% have a relative decrease of 9.5 %, 13.1 %, and 14.4 %, respectively. However, the optical transmittance of the composite prepared from liquid nitrogen freeze-casted cryogel with pectin concentration of 3.0 wt% has a relative decrease of 24.7 % when the thickness increases from 1.3 mm to 3.1 mm. This suggests that cryogel with bigger pores, which is prepared from lower pectin concentration and higher freeze-casting temperature, is more suitable for the preparation of thicker composites with higher optical transmittance.

In addition to the good optical transparent property of these pectin/PMMA composites in the visible light region, the strong absorption in the UV light region at 340 nm of pectin (Fig. 5a) due to its carbonyl groups [54] (which have $n \rightarrow \pi^*$ transitions) indicates that the pectin/PMMA composites have the UV blocking ability. The thickness dependences of UVA (320–400 nm) and UVB (290–320 nm) blocking percentages for pectin/PMMA composites, PMMA and glass are shown in Fig. 5e and 5f, respectively. It is observed that both UVA and UVB block percentages increase with the thickness for all the samples and they increase as well when increasing the pectin concentration. Comparing to pure PMMA, all pectin/PMMA composites have much higher UVA and UVB blocking abilities. Although the UVB blocking ability of pectin/PMMA composites with low pectin concentration is slightly lower than glass, it has similar UVB blocking ability when the pectin concentration reaches 4.5 wt%. UVA blocking ability for all the pectin/PMMA composites is much higher than glass and it is enhanced by increasing the pectin concentration. Interestingly, the pectin concentration and the thickness of the composites have only a minute influence on the transmittance in the visible light region (Fig. 5c) but have

a strong influence on the UV blocking ability (Fig. 5e and 5f). The reason for this is that pectin has weak absorption for visible light and strong absorption for the UV light.

The optical properties of pectin/PMMA composites were compared with reported transparent wood and transparent bamboo as illustrated in Fig. 6a and 6b. The detailed data used for compiling this Figure is collected to Table S2 (Supporting Information). It is observed that the pectin/PMMA composites prepared from dry ice freeze-casted pectin cryogels have comparable optical transmittance and comparable or lower haze compared with most reported transparent woods/bamboo with the similar thickness. The high transmittance and low haze for pectin/PMMA composites is caused by the thinner pore wall ($\approx 0.7 \mu\text{m}$) comparing with that of wood [11] ($\approx 1.5 \mu\text{m}$) and bamboo [53] ($\approx 1.4 \mu\text{m}$) used for preparing transparent woods/bamboo. Although some reported transparent woods could also exhibit high transmittance and low haze, further chemical treatment [13] (such as inner surface functionalization) or extra bleaching step [10], which are environmentally-harmful, are needed prior to the infiltration of polymer. Therefore, the method of using freeze-casted pectin cryogel as the template to fabricate transparent composites is environmentally-friendly and, as shown here, can be artificially controlled through varying pectin concentration and freeze-casting temperature to optimize the final composite's optical property. Additionally, for comparison, Fig. 6c presents the transmittance of pectin/PMMA composites and the cellulose nanofiber (CNF)/PMMA composite prepared from freeze-casted CNF cryogel (detailed information of the preparation and morphology of CNF cryogel and the corresponding composite can be found in supporting information and Fig. S5). It is observed that, even with the higher pectin concentration (4.5 wt%), the pectin/PMMA composite still has higher transmittance (83%) comparing to CNF/PMMA composite (74%) at wavelength of 550 nm. For the UVA and UVB blocking abilities, the pectin/PMMA composite outperforms the CNF/PMMA composite remarkably. For example, with the lower pectin concentration (1.5 wt %), the UVA and UVB block percentages of pectin/PMMA composite are 47.1% and 73.3%, which are higher than CNF/PMMA composite (UVA: 34.9%; UVB: 48.2%). Therefore, pectin is more suitable to fabricate composites with high visible light transmittance and high UV blocking ability than cellulose.

In addition to intriguing optical properties, the thermal insulation capacity of these composites, important for instance for energy-efficient applications, was also assessed. The thermal conductivities of pectin/PMMA composites prepared from dry ice freeze-casted cryogels with different pectin concentrations (1.5 wt%-4.5 wt%) were compared with glass, PMMA, and transparent wood/bamboo as shown in Fig. 7a. The thermal conductivities of all pectin/PMMA composites are approximately 7 times lower than glass. They are also lower than the pure PMMA and reported transparent wood [10,18,55,56]/bamboo [53]. Note, pectin/PMMA composites have higher thermal conductivity than

the non-infiltrated freeze-casted cryogels that have thermal conductivity around $0.020 \text{ W}/(\text{m}\cdot\text{K})$ - $0.025 \text{ W}/(\text{m}\cdot\text{K})$. This is due to that the solid PMMA filling the pores could facilitate the heat transfer as compared to air. In addition, the thermal insulation performance of glass, pure PMMA, and pectin/PMMA composites prepared with different freezing method, freeze-casting temperature, and pectin concentration, are further demonstrated by placing samples of equal thickness on a hot plate and measuring their surface temperature by infrared camera (Fig. 7b, 7c and S6). All 2 mm thick samples were placed on a hot plate with temperature maintaining at 80°C . Infrared images of the sample surface were recorded every 10 s after placing each sample on the hot plate (Fig. 7b and S6a, Supporting Information). The surface temperature as a function of heating time for each sample is summarized in Fig. 7c and S6b. After heating 60 s, the surface temperature increases from 27°C to 64°C for all the dry ice freeze-casted pectin/PMMA composites (Fig. 7c). In comparison, the surface temperatures of glass and PMMA are around 75°C and 70°C , respectively, after heating 60 s (Fig. 7c). Meanwhile, it reaches 60°C much faster comparing to the dry ice freeze-casted pectin/PMMA composites. This is due to the stronger phonon scattering [57,58] at the interface between pectin pore wall and PMMA (Fig. 7d). Similar explanation was also proposed by Li et al. for the transparent wood [55]. However, for the liquid nitrogen freeze-casted and randomly frozen pectin/PMMA composites, the surface temperature can reach 66°C and 68°C , respectively. These values locate in between glass (or PMMA) and dry ice freeze-casted pectin/PMMA composites. Therefore, dry ice freeze-casted pectin/PMMA composites have better thermal insulation property than glass, PMMA, and pectin/PMMA composites prepared from liquid nitrogen freeze-casted cryogel and randomly frozen cryogel, and they could be used for energy-efficient applications.

4. Conclusion

A novel class of optically transparent pectin/PMMA composite with improved thermal insulation ability has been prepared by the infiltration of PMMA into freeze-casted pectin cryogels. Pectin cryogels fabricated via freeze-casting method have an anisotropic structure which endows the corresponding composites with an anisotropic light scattering and higher optical transmittance as compared to that of the composite prepared from randomly frozen pectin cryogel. These pectin/PMMA composites have comparable optical transmittance and comparable or lower haze than that of most reported transparent wood/bamboo with the similar thickness. Meanwhile, this type of composite has very good UV blocking ability as compared to conventional glass, pure PMMA, and nanocellulose composites. Moreover, wide range of optical properties can be produced via controlling the pectin concentration and freeze-casting temperature. The high optical transmittance of 84% and low haze of 38% were achieved for 1.3 mm thick pectin/

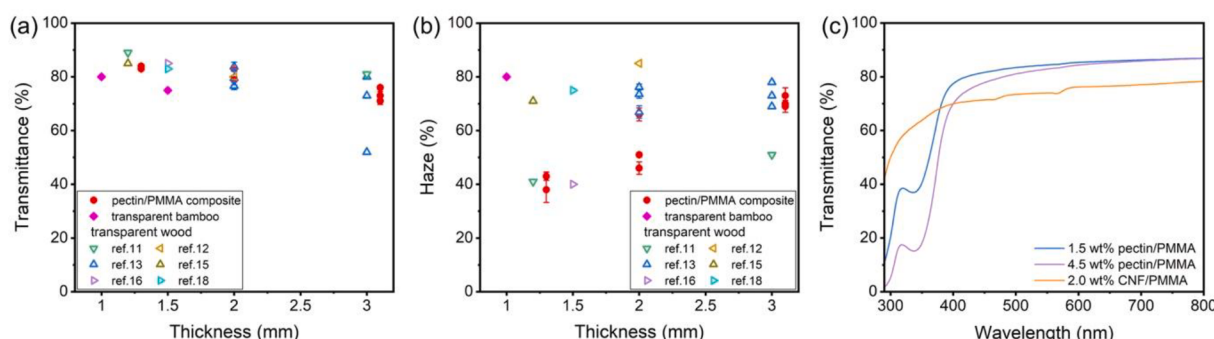


Fig. 6. Comparison of pectin/PMMA composites with reported transparent wood [11–13,15,16,18] and transparent bamboo [53] for their optical transmittance (a) and haze (b) at wavelength of 550 nm. (c) Optical transmittance of the 1.3 mm thick pectin/PMMA composite sheets prepared from dry ice freeze-casted cryogels with 1.5 wt% and 4.5 wt% pectin concentrations and 1.3 mm thick CNF/PMMA composite sheet prepared from liquid nitrogen freeze-casted cryogels with 2.0 wt% CNF concentration (diluted from 2.3 wt% CNF suspension which is produced in Aalto University). If the errors are not seen, they are smaller or equal to the symbol.

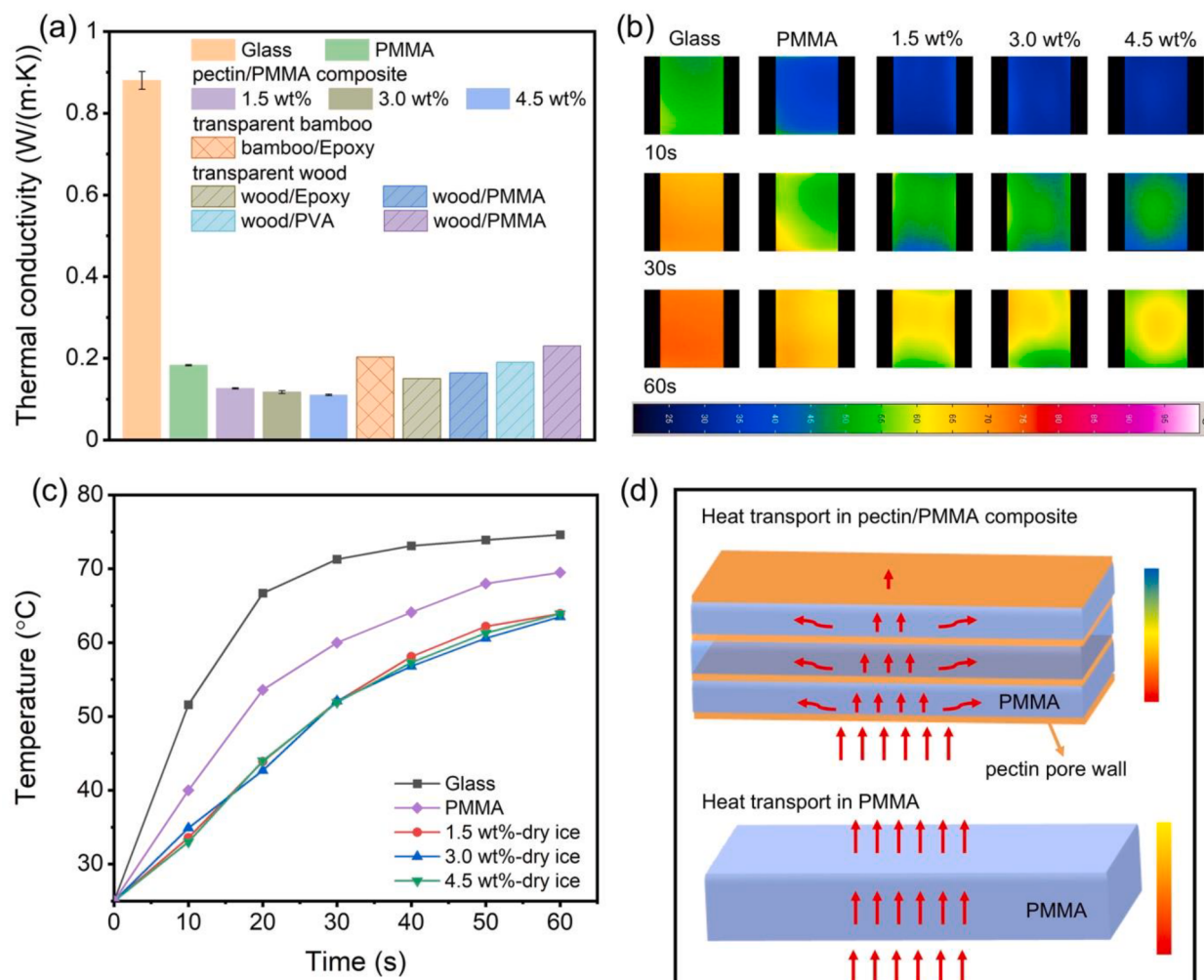


Fig. 7. Thermal conductivity of glass, pectin/PMMA composites prepared from dry ice freeze-casted cryogels, and reported transparent wood [10,18,55,56]/bamboo [53] (a). Representative infrared thermal images in the heating process (b) and the relevant maximum surface temperature as function of heating time (c) for the 2 mm thick glass, PMMA, and pectin/PMMA composite sheets prepared from dry ice freeze-casted cryogels with different pectin concentration solutions. The schematic illustration of heat transport in pectin/PMMA composite and pure PMMA (d). If the errors are not seen, they are smaller or equal to the symbol.

PMMA composite prepared from dry ice freeze-casted pectin cryogel with pectin concentration of 1.5 wt%. Optical transmittance decreases with increasing pectin concentration and thickness, and with decreasing freeze-casting temperature. On the other hand, haze increases with increasing the thickness, and with decreasing freeze-casting temperature in most cases. Furthermore, the studied pectin/PMMA composite has better thermal insulation property than glass and PMMA. Therefore, these pectin/PMMA composites provide an optimized combination of functionalities including optical transparency, UV blocking, and thermal insulation, which could turn out to be useful in optical and energy-efficient applications.

Declaration of Competing Interest

The authors declare that they have no known competing financial interests or personal relationships that could have appeared to influence the work reported in this paper.

Acknowledgments

This work was supported by the Academy of Finland projects "SUBSTAINABLE" (Decision number 334818) and "SUPER-WEAR" (decision number: 322214). We acknowledge BioEconomy and Raw-MatTERS Finland infrastructure (RAMI) facilities based at Aalto

University for measurements.

Appendix A. Supplementary data

Supplementary data to this article can be found online at <https://doi.org/10.1016/j.cej.2022.135738>.

References

- [1] X. Zhang, X. Zhao, T. Xue, F. Yang, W. Fan, T. Liu, Bidirectional anisotropic polyimide/bacterial cellulose aerogels by freeze-drying for super-thermal insulation, *Chem. Eng. J.* 385 (2020), 123963, <https://doi.org/10.1016/j.cej.2019.123963>.
- [2] F. Zou, T. Budtova, Polysaccharide-based aerogels for thermal insulation and superinsulation: An overview, *Carbohydr. Polym.* 266 (2021), 118130, <https://doi.org/10.1016/j.carbpol.2021.118130>.
- [3] F. Hu, S. Wu, Y. Sun, Hollow-Structured Materials for Thermal Insulation, *Adv. Mater.* 31 (2019) 1801001, <https://doi.org/10.1002/adma.201801001>.
- [4] P. Xue, S. Liu, X. Shi, C. Sun, C. Lai, Y. Zhou, D. Sui, Y. Chen, J. Liang, A hierarchical silver-nanowire-graphene host enabling ultrahigh rates and superior long-term cycling of lithium-metal composite anodes, *Adv. Mater.* 30 (2018) 1804165, <https://doi.org/10.1002/adma.201804165>.
- [5] Y.C. Yin, Z.L. Yu, Z.Y. Ma, T.W. Zhang, Y.Y. Lu, T. Ma, F. Zhou, H. Bin Yao, Y. Shu-Hong, Bio-inspired low-tortuosity carbon host for high-performance lithium-metal anode, *Natl. Sci. Rev.* 6 (2019) 247–256, <https://doi.org/10.1093/nsr/nwy148>.
- [6] X. Zhang, Z. Ju, L.M. Housel, L. Wang, Y. Zhu, G. Singh, N. Sadique, K.J. Takeuchi, E.S. Takeuchi, A.C. Marschilok, G. Yu, Promoting Transport Kinetics in Li-Ion Battery with Aligned Porous Electrode Architectures, *Nano Lett.* 19 (2019) 8255–8261, <https://doi.org/10.1021/acs.nanolett.9b03824>.

- [7] C. Wang, X. Chen, B. Wang, M. Huang, B. Wang, Y. Jiang, R.S. Ruoff, Freeze-Casting Produces a Graphene Oxide Aerogel with a Radial and Centrosymmetric Structure, *ACS Nano* 12 (2018) 5816–5825, <https://doi.org/10.1021/acsnano.8b01747>.
- [8] J. Yang, Y. Xia, P. Xu, B. Chen, Super-elastic and highly hydrophobic/superoleophilic sodium alginate/cellulose aerogel for oil/water separation, *Cellulose* 25 (2018) 3533–3544, <https://doi.org/10.1007/s10570-018-1801-8>.
- [9] T. Liu, M. Huang, X. Li, C. Wang, C.X. Gui, Z.Z. Yu, Highly compressible anisotropic graphene aerogels fabricated by directional freezing for efficient absorption of organic liquids, *Carbon* 100 (2016) 456–464, <https://doi.org/10.1016/j.carbon.2016.01.038>.
- [10] R. Mi, T. Li, D. Dalgo, C. Chen, Y. Kuang, S. He, X. Zhao, W. Xie, W. Gan, J. Zhu, J. Srebric, R. Yang, L. Hu, A. Clear, Strong, and Thermally Insulated Transparent Wood for Energy Efficient Windows, *Adv. Funct. Mater.* 30 (2020) 1907511, <https://doi.org/10.1002/adfm.201907511>.
- [11] C. Montanari, Y. Ogawa, P. Olsén, L.A. Berglund, High Performance, Fully Bio-Based, and Optically Transparent Wood Biocomposites, *Adv. Sci.* 8 (2021) 2100559, <https://doi.org/10.1002/advs.202100559>.
- [12] M. Zhu, J. Song, T. Li, A. Gong, Y. Wang, J. Dai, Y. Yao, W. Luo, D. Henderson, L. Hu, Highly Anisotropic, Highly Transparent Wood Composites, *Adv. Mater.* 28 (2016) 5181–5187, <https://doi.org/10.1002/adma.201600427>.
- [13] C. Montanari, P. Olsén, L.A. Berglund, Interface tailoring by a versatile functionalization platform for nanostructured wood biocomposites, *Green Chem.* 22 (2020) 8012–8023, <https://doi.org/10.1039/d0gc02768e>.
- [14] Y. Liu, H. Yang, C. Ma, S. Luo, M. Xu, Z. Wu, W. Li, S. Liu, Luminescent Transparent Wood Based on Lignin-Derived Carbon Dots as a Building Material for Dual-Channel, Real-Time, and Visual Detection of Formaldehyde Gas, *ACS Appl. Mater. Interfaces* 12 (2020) 36628–36638, <https://doi.org/10.1021/acsmi.0c10240>.
- [15] Y. Li, Q. Fu, S. Yu, M. Yan, L. Berglund, Optically Transparent Wood from a Nanoporous Cellulosic Template: Combining Functional and Structural Performance, *Biomacromolecules* 17 (2016) 1358–1364, <https://doi.org/10.1021/acsm.biomac.6b00145>.
- [16] C. Jia, C. Chen, R. Mi, T. Li, J. Dai, Z. Yang, Y. Pei, S. He, H. Bian, S.H. Jang, J. Y. Zhu, B. Yang, L. Hu, Clear Wood toward High-Performance Building Materials, *ACS Nano* 13 (2019) 9993–10001, <https://doi.org/10.1021/acsnano.9b00089>.
- [17] Y. Li, E. Vasileva, I. Sychugov, S. Popov, L. Berglund, Optically Transparent Wood: Recent Progress, Opportunities, and Challenges, *Adv. Opt. Mater.* 6 (2018) 1800059, <https://doi.org/10.1002/adom.201800059>.
- [18] Y. Li, Q. Fu, R. Rojas, M. Yan, M. Lawoko, L. Berglund, Lignin-Retaining Transparent Wood, *ChemSusChem* 10 (2017) 3445–3451, <https://doi.org/10.1002/cssc.201701089>.
- [19] Q. Xia, C. Chen, T. Li, S. He, J. Gao, X. Wang, L. Hu, Solar-assisted fabrication of large-scale, patternable transparent wood, *Sci. Adv.* 7 (2021) 1–9, <https://doi.org/10.1126/sciadv.abd7342>.
- [20] R. Mi, C. Chen, T. Keplinger, Y. Pei, S. He, D. Liu, J. Li, J. Dai, E. Hitz, B. Yang, I. Burgert, L. Hu, Scalable aesthetic transparent wood for energy efficient buildings, *Nat. Commun.* 11 (2020) 3836, <https://doi.org/10.1038/s41467-020-17513-w>.
- [21] U. Müller, M. Rätzsch, M. Schwanninger, M. Steiner, H. Zöbl, Yellowing and IR-changes of spruce wood as result of UV-irradiation, *J. Photochem. Photobiol. B Biol.* 69 (2003) 97–105, [https://doi.org/10.1016/S1011-1344\(02\)00412-8](https://doi.org/10.1016/S1011-1344(02)00412-8).
- [22] Y. Li, X. Yang, Q. Fu, R. Rojas, M. Yan, L. Berglund, Towards centimeter thick transparent wood through interface manipulation, *J. Mater. Chem. A* 6 (2018) 1094–1101, <https://doi.org/10.1039/c7ta09973h>.
- [23] P.D. Determinations, Density adsorption permeability, *J. Phys. Chem.* 33 (1929) 398–414.
- [24] G. Shao, D.A.H. Hanaor, X. Shen, A. Gurlo, Freeze Casting: From Low-Dimensional Building Blocks to Aligned Porous Structures—A Review of Novel Materials, Methods, and Applications, *Adv. Mater.* 32 (2020) 1907176, <https://doi.org/10.1002/adma.201907176>.
- [25] C. Lei, Z. Xie, K. Wu, Q. Fu, Controlled Vertically Aligned Structures in Polymer Composites: Natural Inspiration, Structural Processing, and Functional Application, *Adv. Mater.* 33 (49) (2021) 2103495.
- [26] J. Han, G. Du, W. Gao, H. Bai, An Anisotropically High Thermal Conductive Boron Nitride/Epoxy Composite Based on Nacre-Mimetic 3D Network, *Adv. Funct. Mater.* 29 (2019) 1900412, <https://doi.org/10.1002/adfm.201900412>.
- [27] B. Wicklein, A. Kocjan, G. Salazar-Alvarez, F. Carosio, G. Camino, M. Antonietti, L. Bergström, Thermally insulating and fire-retardant lightweight anisotropic foams based on nanocellulose and graphene oxide, *Nat. Nanotechnol.* 10 (2015) 277–283, <https://doi.org/10.1038/nnano.2014.248>.
- [28] Z.Z. Pan, H. Nishihara, S. Iwamura, T. Sekiguchi, A. Sato, A. Isogai, F. Kang, T. Kyotani, Q.H. Yang, Cellulose Nanofiber as a Distinct Structure-Directing Agent for Xylem-like Microhoneycomb Monoliths by Unidirectional Freeze-Drying, *ACS Nano* 10 (2016) 10689–10697, <https://doi.org/10.1021/acsnano.6b05808>.
- [29] W. Xiao, P. Wang, X. Song, B. Liao, K. Yan, J.J. Zhang, Facile Fabrication of Anisotropic Chitosan Aerogel with Hydrophobicity and Thermal Superinsulation for Advanced Thermal Management, *ACS Sustain. Chem. Eng.* 9 (2021) 9348–9357, <https://doi.org/10.1021/acssuschemeng.1c02217>.
- [30] J. Zhu, R. Xiong, F. Zhao, T. Peng, J. Hu, L. Xie, H. Xie, K. Wang, C. Jiang, Lightweight, High-Strength, and Anisotropic Structure Composite Aerogel Based on Hydroxyapatite Nanocrystal and Chitosan with Thermal Insulation and Flame Retardant Properties, *ACS Sustain. Chem. Eng.* 8 (2020) 71–83, <https://doi.org/10.1021/acssuschemeng.9b03953>.
- [31] M. Zhang, S. Jiang, F. Han, M. Li, N. Wang, L. Liu, Anisotropic cellulose nanofiber/chitosan aerogel with thermal management and oil absorption properties, *Carbohydr. Polym.* 264 (2021), 118033, <https://doi.org/10.1016/j.carbpol.2021.118033>.
- [32] Y. Zhou, S. Fu, Y. Pu, S. Pan, A.J. Ragauskas, Preparation of aligned porous chitin nanowhisker foams by directional freeze-casting technique, *Carbohydr. Polym.* 112 (2014) 277–283, <https://doi.org/10.1016/j.carbpol.2014.05.062>.
- [33] J. Shan, D. Liu, F. Su, M. Li, H. Tian, M. Guo, W. Qiao, J. He, Q. Li, J. Qian, Anisotropic Structure and Properties of Chitin and Chitosan Nanofibril-Supported Starch Foams, *ACS Sustain. Chem. Eng.* 8 (2020) 17387–17396, <https://doi.org/10.1021/acssuschemeng.0c05484>.
- [34] K. Qiu, U.G.K. Wegst, Excellent Specific Mechanical and Electrical Properties of Anisotropic Freeze-Cast Native and Carbonized Bacterial Cellulose-Alginate Foams, *Adv. Funct. Mater.* 32 (1) (2022) 2105635.
- [35] A. Pettignano, N. Tanchoux, T. Cacciaguerra, T. Vincent, L. Bernardi, E. Guibal, F. Quignard, Sodium and acidic alginate foams with hierarchical porosity: Preparation, characterization and efficiency as a dye adsorbent, *Carbohydr. Polym.* 178 (2017) 78–85, <https://doi.org/10.1016/j.carbpol.2017.09.022>.
- [36] H.K. Chang, C.W. Huang, C.C. Chiu, H.J. Wang, P.Y. Chen, Fabrication of anisotropic poly(vinyl alcohol) scaffolds with controllable mechanical properties and structural recoverability under compression via a freeze-casting technique, *Macromolecules* 53 (2020) 8809–8818, <https://doi.org/10.1021/acs.macromol.0c01608>.
- [37] S. Christoph, A. Hamraoui, E. Bonnin, C. Garnier, T. Coradin, F.M. Fernandes, Ice-templating beet-root pectin foams: Controlling texture, mechanics and capillary properties, *Chem. Eng. J.* 350 (2018) 20–28, <https://doi.org/10.1016/j.cej.2018.05.160>.
- [38] T. Nissilä, M. Hietala, K. Oksman, A method for preparing epoxy-cellulose nanofiber composites with an oriented structure, *Compos. Part A Appl. Sci. Manuf.* 125 (2019), 105515, <https://doi.org/10.1016/j.compositesa.2019.105515>.
- [39] T. Zhai, Q. Zheng, Z. Cai, L.S. Tung, H. Xia, S. Gong, Poly(vinyl alcohol)/cellulose nanofibril hybrid aerogels with an aligned microtubular porous structure and their composites with polydimethylsiloxane, *ACS Appl. Mater. Interfaces* 7 (2015) 7436–7444, <https://doi.org/10.1021/acsami.5b01679>.
- [40] T. Nissilä, S.S. Karhula, S. Saarakkala, K. Oksman, Cellulose nanofiber aerogels impregnated with bio-based epoxy using vacuum infusion: Structure, orientation and mechanical properties, *Compos. Sci. Technol.* 155 (2018) 64–71, <https://doi.org/10.1016/j.compsitech.2017.12.001>.
- [41] W.G.T. Willats, J.P. Knox, J.D. Mikkelsen, Pectin: New insights into an old polymer are starting to gel, *Trends Food Sci. Technol.* 17 (2006) 97–104, <https://doi.org/10.1016/j.tifs.2005.10.008>.
- [42] P. Ishwarya S, S. R, P. Nisha, Advances and prospects in the food applications of pectin hydrogels, *Crit. Rev. Food Sci. Nutr.* (2021). <https://doi.org/10.1080/10408398.2021.1875394>.
- [43] M.C.N. Picot-Alain, B. Ramasawmy, M.N. Emmambux, Extraction, Characterisation, and Application of Pectin from Tropical and Sub-Tropical Fruits: A Review, *Food Rev. Int.* 38 (3) (2022) 282–312.
- [44] M.T. Tunç, H.I. Odabaş, Single-step recovery of pectin and essential oil from lemon waste by ohmic heating assisted extraction/hydrodistillation: A multi-response optimization study, *Innov. Food Sci. Emerg. Technol.* 74 (2021), 102850, <https://doi.org/10.1016/j.ifset.2021.102850>.
- [45] C. He, I. Sampers, K. Raes, Isolation of Pectin from Clementine Peel: A New Approach Based on Green Extracting Agents of Citric Acid/Sodium Citrate Solutions, *ACS Sustain. Chem. Eng.* 9 (2021) 833–843, <https://doi.org/10.1021/acssuschemeng.0c07422>.
- [46] L.H. Reichembach, C. Lúcia de Oliveira Petkowicz, Pectins from alternative sources and uses beyond sweets and jellies: An overview, *Food Hydrocoll.* 118 (2021) 106824, <https://doi.org/10.1016/j.foodhyd.2021.106824>.
- [47] S. Groult, T. Budtova, Thermal conductivity/structure correlations in thermal super-insulating pectin aerogels, *Carbohydr. Polym.* 196 (2018) 73–81, <https://doi.org/10.1016/j.carbpol.2018.05.026>.
- [48] X. Niu, Y. Liu, G. Fang, C. Huang, O.J. Rojas, H. Pan, Highly Transparent, Strong, and Flexible Films with Modified Cellulose Nanofiber Bearing UV Shielding Property, *Biomacromolecules* 19 (2018) 4565–4575, <https://doi.org/10.1021/acs.biomac.8b01252>.
- [49] K. Krichbaum, P. Munier, V. Apostolopoulou-Kalkavoura, N. Lavoine, Analysis of the Porous Architecture and Properties of Anisotropic Nanocellulose Foams: A Novel Approach to Assess the Quality of Cellulose Nanofibrils (CNFs), *ACS Sustain. Chem. Eng.* 6 (2018) 11959–11967, <https://doi.org/10.1021/acssuschemeng.8b02278>.
- [50] B. Chen, Q. Zheng, J. Zhu, J. Li, Z. Cai, L. Chen, S. Gong, Mechanically strong fully biobased anisotropic cellulose aerogels, *RSC Adv.* 6 (2016) 96518–96526, <https://doi.org/10.1039/c6ra19280g>.
- [51] K. Nikolova, I. Panchev, S. Sainov, Optical characteristics of biopolymer films from pectin and gelatin, *J. Optoelectron. Adv. Mater.* 7 (2005) 1439–1444.
- [52] H. Chen, A. Baitenov, Y. Li, E. Vasileva, S. Popov, I. Sychugov, M. Yan, L. Berglund, Thickness Dependence of Optical Transmittance of Transparent Wood: Chemical Modification Effects, *ACS Appl. Mater. Interfaces* 11 (2019) 35451–35457, <https://doi.org/10.1021/acsami.9b11816>.
- [53] X. Wang, S. Shan, S.Q. Shi, Y. Zhang, L. Cai, L.M. Smith, Optically Transparent Bamboo with High Strength and Low Thermal Conductivity, *ACS Appl. Mater. Interfaces* 13 (2021) 1662–1669, <https://doi.org/10.1021/acsami.0c21245>.
- [54] H. Kaczmarek, A. Dabrowska, I. Vuković-Kwiatkowska, Accelerated weathering of pectin/poly(vinyl alcohol) blends studied by spectroscopic methods, *J. Appl. Polym. Sci.* 122 (2011) 1936–1945, <https://doi.org/10.1002/app.34298>.
- [55] T. Li, M. Zhu, Z. Yang, J. Song, J. Dai, Y. Yao, W. Luo, G. Pastel, B. Yang, L. Hu, Wood Composite as an Energy Efficient Building Material: Guided Sunlight Transmittance and Effective Thermal Insulation, *Adv. Energy Mater.* 6 (2016) 1601122, <https://doi.org/10.1002/aenm.201601122>.

- [56] X. Wang, T. Zhan, Y. Liu, J. Shi, B. Pan, Y. Zhang, L. Cai, S.Q. Shi, Large-Size Transparent Wood for Energy-Saving Building Applications, *ChemSusChem* 11 (2018) 4086–4093, <https://doi.org/10.1002/cssc.201801826>.
- [57] S. Hida, T. Hori, T. Shiga, J. Elliott, J. Shiomi, Thermal resistance and phonon scattering at the interface between carbon nanotube and amorphous polyethylene, Int. J. Heat Mass Transf. 67 (2013) 1024–1029, <https://doi.org/10.1016/j.ijheatmasstransfer.2013.08.068>.
- [58] X. Yan, W. Liu, H. Wang, S. Chen, J. Shiomi, K. Esfarjani, H. Wang, D. Wang, G. Chen, Z. Ren, Stronger phonon scattering by larger differences in atomic mass and size in p-type half-Heuslers $\text{Hf}_{1-x}\text{TixCoSb}_{0.8}\text{Sn}_{0.2}$, *Energy Environ. Sci.* 5 (2012) 7543–7548, <https://doi.org/10.1039/c2ee21554c>.